We are IntechOpen, the world's leading publisher of Open Access books Built by scientists, for scientists

4,800
Open access books available

122,000
International authors and editors

135M
Downloads

Our authors are among the

154
Countries delivered to

TOP 1%
most cited scientists

12.2%
Contributors from top 500 universities

CLARIVATE ANALYTICS BOOK CITATION INDEX INDEXED

WEB OF SCIENCE™

Selection of our books indexed in the Book Citation Index in Web of Science™ Core Collection (BKCI)

Interested in publishing with us?
Contact book.department@intechopen.com

Numbers displayed above are based on latest data collected.
For more information visit www.intechopen.com

Chapter 3

Fundamentals of Plasma-Material Interactions in Magnetic Fusion Devices

Jean Paul Allain and David N. Ruzic

Additional information is available at the end of the chapter

http://dx.doi.org/10.5772/intechopen.77157

Abstract

The interaction of plasmas and materials has a long history in the modification of condensed matter. Plasma-material interaction (PMI) can govern how low-temperature and high-temperature plasmas interact and modify materials surfaces. In magnetic fusion devices, PMI can also influence the operation of the fusion device. For example, incident energetic charged particle on fusion wall material surfaces can release target atoms via sputtering and can implant fuel particles in the lattice. Implanted energetic particles can mix fuel and influence recycling of fuel back to the plasma. Sputtered target atoms can become ionized in the magnetic sheath and re-deposit at the wall surface. The magnetic sheath will influence the energy and angular distribution of incident energetic particles and influence the implantation and release of fusion fuel.

Keywords: plasma-material interactions, sputtering, reflection, retention, magnetic sheath

1. Introduction

The interaction of plasmas and materials is one of the most interesting and critical subjects in the field of plasma technology. In fact, plasma processing has been the hallmark of plasma technology and its impact on the semiconductor industry. Plasmas are ubiquitous in nature and are responsible for some of the most fundamental interactions known to man. For example, in astrobiology, the early formation of the stars from interstellar media (ISM) dust and the presence of hydrogen molecules in interstellar space are conjectured to be governed by carbonaceous dust grain surface interactions with plasma energetic particles (hydrogen, helium) forming more complex organic molecules [1, 2]. Ion-induced etching in modern high-density plasma-processing tools is driven by the complex energetic multi-particle interaction with

material surfaces, and fluorescent lamps operate by a balance of the plasma-material interaction (PMI) under high gas pressure containers.

Fusion reactors also witness significant modification of wall materials when exposed to high-density high-temperature magnetized plasmas. The nuclear fusion reaction in the core plasma generates a plethora of energetic particles including He and neutrons for hydrogen-based fuels. Both highly energetic He and neutrons can penetrate deep inside the material structure. However, the charged particles that remain inside the reactor are controlled by the boundary plasma with the reactor wall, and through what is known as a magnetic sheath, the charged particles are driven to the surface by several mechanisms that dictate both their incidence angle and energy to the material surface. Fusion devices are only experimental and operate under a pulsating configuration that enables only pulsed fusion plasmas that range from a few seconds up to about 50–60 s for the most modern, super-conducting fusion devices. During the pulse, the plasma can drive many complex interactions at the plasma edge and at the wall surface can implant energetic particles that range from a few eV up to several kilo-electron volts (keV). These energetic particles are mostly fuel particles such as hydrogen or deuterium but also in some cases helium. Other particles are mostly impurities from the ambient (e.g., water) such as oxygen and material atoms sputtered and re-deposited in the fusion device. In this chapter, we examine in detail the interactions of these energetic particles and material surfaces to understand the basic mechanisms that drive plasma-material interactions.

Beyond energetic particle interaction on the wall material surface, there are additional complex interactions that take place and evolve during plasma-material interaction. The surface kinetics of impurity-driven modification can change the surface chemistry and morphology significantly. Over time, fusion devices also can drive transient events that consist of instabilities from the plasma, releasing large amounts of energy in the form of heat to the wall material surface. In a fusion reactor, deuterium-tritium plasma is confined by strong magnetic fields at a temperature of hundreds of millions of degrees Celsius. Therefore, in the exhaust of such a reactor, the so-called divertor, the plasma-facing surfaces are subjected to extremely high and intermittent heat loads (10 MW/m^2 time-averaged, with periodic excursions in the GW/m^2 level on sub-millisecond timescales), while simultaneously being bombarded by extreme fluxes of energetic particles (hydrogen isotopes, helium, neutrons). The radiation interaction with matter will be dynamic, imposing time-dependent changes on the structure, composition, and chemistry of both bulk and surface region of material components. Performance and lifetime limits of nuclear fusion materials will ultimately need to survive >100-dpa and >1000-appm He production over the high-duty cycle operation of the reactor. Currently, no material can meet such requirements namely limited by critical material properties including creep resistance, fracture toughness, surface erosion/re-deposition, corrosion, chemistry, thermal conductivity, and many others.

Although progress has been made in the last decade in establishing an understanding of plasma-material interactions, there remain critical knowledge gaps as it relates to predicting and designing for the behavior at the plasma-material interface under the so-called "reactor-relevant" plasma conditions anticipated in a future plasma-burning neutron-dominated environment. Ultimately, a magnetically confined fusion plasma must be able to not only operate

under "burn" conditions (e.g., more power out than power in) but when used to generate electricity operate at high-duty cycles (e.g., weeks or months of continuous power).

The plasma-material interface is one important factor to the realization of nuclear fusion power. At this interface, high particle and heat flux from the fusion plasma can limit the material's lifetime and reliability and therefore hinder operation of the fusion device. This region is critical to the operation of a nuclear fusion reactor since material can be emitted both atomistically (e.g., evaporation, sputtering, etc.) and/or macroscopically (i.e., during transient events, such as disruptions or edge-localized modes). The environmental conditions of a future nuclear fusion reactor interacting with the plasma-material interface are extreme. The incident plasma will carry heat fluxes of the order of hundreds of MWm^{-2} and particle fluxes that can average 10^{24} m^{-2} s^{-1}. The fusion reactor wall would need to operate at high temperatures near 800°C, and the incident energy of particles will vary from a few eV ions to MeV neutrons. To exacerbate this, another challenge is the management of damage over the course of time. Operating at reactor-relevant conditions means the wall material would need to perform over the course of not just seconds or minutes (i.e., as in most advanced fusion devices today and the near future) but months to years. Therefore, plasma-material interface is a dynamic, evolving, reconstituted region of material that is constantly eroded and re-deposited a million times over rendering our current understanding of material damage quite limited.

Another important factor is the limited attention given not only to the structural properties of refractory metals such as tungsten but especially surface-dominating properties (e.g., erosion, ion mixing, hydrogen- and helium-induced bubbles and swelling at the surface, surface diffusion, surface chemistry, morphology, and nanoscale patterning) that ultimately dictate particle recycling emitted back to the edge plasma consequently cooling the fusion plasma. In addition, understanding the relevant plasma-facing component issues, which vary with respect to fusion device design, is also lacking in fusion material's R&D efforts. For example, the differences of plasma edge conditions for first wall versus divertor fusion materials are quite different. Incident He fluxes to the first wall of future plasma-burning devices may vary between 10^{18} and 10^{19} m^{-2} s^{-1} and energies 100 and 1000 eV and at the divertor, fluxes between 10^{22} and 10^{23} m^{-2} s^{-1} and energies 5 and 100 eV. These flux and energy regimes induce distinct damage mechanisms that must be understood in the development of advanced fusion materials. Of the various material options at the plasma-material interface (i.e., graphite, liquid metals, etc.), refractory metals (molybdenum, tungsten, etc.) are attractive for use during steady-state, high-temperature (700–1000°C) operation with heat flux ranging between 10 and 20 MW/m^2. However, one major challenge for the application of solid refractory metals in future burning plasmas is the large production of helium ash in a fusion reactor. He implantation and generation of cavities, bubbles, surface morphology (e.g., fuzz), and blisters is of major concern for the application of commercial-grade tungsten materials. The surface nano- and mesoscale morphology could be detrimental to the performance of nuclear fusion reactor operation given the possible micro- and macroscale emission of W particulate (dust) into the plasma.

Given the broad area of plasma-material interactions and its importance to many different disciplines, we limit our treatment in this chapter to the interactions and plasmas in magnetic fusion devices. We also limit our coverage of PMI to one specific set of mechanisms mainly focused on physical sputtering and incident-particle reflection.

2. PMI basics

The basic interaction of a plasma bounded by a material surface is the balance of charged particles that arrive at a given time. In a magnetized plasma, the incident ions gyro-orbit around magnetic field lines that intersect material surfaces at ultra-shallow angles between 1 and 3° with respect to the surface, resulting in the so-called "Chodura sheath" where incident ions arrive with a distribution of incident angles and energies ranging from 20 to 60° with respect to surface normal and energies between 10 and 100 eV, respectively. The incident ions (mostly hydrogen fuel particles) implant at depths between a few nm to hundreds of nm. Sputtering of the wall material will depend on these conditions for both light and heavy mass target materials. The incident hydrogen particles will also reflect or backscatter from the surface and carry a finite amount of energy also resulting in a balance of implanted versus recycled fuel particles in a fusion device. In this section, we briefly discuss some of the most salient sputtering and reflection mechanisms with realistic (e.g., rough) surfaces found in a fusion device.

2.1. Ion-surface interactions

Ion-surface interactions are one of the most important effects in fusion research devices. Open field lines terminate at divertor plates or strike walls at very grazing angles. The ion trajectories, which spiral around these field lines, direct energetic ions onto the wall material. Therefore, ion-solid and more recently ion-liquid interactions are the critical reaction at the boundary and therefore the most important to understand. The incident ion could reflect back into the plasma or could become embedded in the surface. Perhaps more importantly, the ion could knock some of the wall material into the plasma, thus leading to sputtering. Since sputtered species are usually electrically neutral, they ignore magnetic field lines and can penetrate a significant distance into the plasma before becoming ionized. Therefore, the energy and angular distribution of sputtered material becomes crucial to predicting edge plasma behavior, and the behavior of the edge plasma is often a controlling factor on the behavior of the core plasma. The interaction of energetic ions with wall materials can also result in not only erosion and re-deposition of post-ionized material wall particles but also could drive composition and morphology changes that over time significantly affect materials' surface properties. Both composition and morphology changes on the surface can result in significant changes both to the plasma-material interactions and consequently to the plasma edge, which can have effects on the core plasma performance.

2.2. Simulating ion-surface interactions

The number of variables that could go into a single ion-surface interaction is numerous. Consider the incident ion. What is its mass, its atomic number, its energy? What angle does it strike the surface with respect to the surface normal? Now, consider the target material. What is its composition, and how does that composition vary with depth? What does the surface roughness look like and at what scale lengths? What is the chemical binding energy of the variety of constituents that may be present, and with what energy is each constituent bound to

each other? The information we wish to know has many facets as well. What species is liberated? What is its energy? What angle does it leave the surface with respect to the surface normal and with respect to the incoming trajectory? Does it come off as a neutral, an ion, a dimer, or a molecule? With so many variables, exhaustive experimental determination of these quantities is impossible. What is possible is a computer model based on the physics of the interactions and then tested against experimental data. If a model can be shown to agree with experiments over a wide variety of ion-target pairs, there is some confidence that it will accurately predict PMI variables even for situations that may be impossible to directly measure. Such a computer scheme exists—Monte-Carlo simulations based on a binary collision approximation. Monte-Carlo simulations are ideal for ion-surface interactions. The physics of any one interaction is straightforward. Stringing many together while randomizing the impact parameter according to the physical parameters of the situation can be done with relative ease. Both the incident particle and all particles, which receive more than some pre-set amount of kinetic energy, are then followed after the collision. After every particle in this cascade is tracked until they come to rest or leave the surface, the final location and velocity of each atom is recorded. The transport of ions in matter (TRIM) simulation code has been one of the most successful PMI codes to simulate the interaction of energetic particles with surfaces and in the context of PMI-simulating effects such as ion implantation and sputtering [3].

2.3. Effects of roughness on PMI

Expanding from the successful TRIM simulation platform, many variances have emerged over many decades and one of them is the incorporation of fractal geometry to mimic realistic surfaces [4].

Figure 1a shows the reflection of 50 eV H from an Ni surface as a function of fractal dimension [5]. R_n is the fraction of particles that reflect and R_e is the fraction of energy that is reflected. Note the precipitous drop in both R_n and R_e when some roughness is added, especially when the incident particle strikes the surface at a grazing incidence (75° from the normal). Initially, roughness reduces reflection as expected. The gradual rise in reflection for very rough surfaces is attributed to there being less of a chance for an upward-moving atom to be recaptured due to the lower average density of the material near the surface. Planar TRIM is akin to the D = 2.00 case for normal incidence. Some interesting comparisons [4] are shown in **Figure 1b**. Here, D is fixed at 2.30 and planar TRIM is compared to fractal TRIM (FTRIM) for three different incident energies as a function of incident angle. Specular reflection tendencies are clearly seen with TRIM but not in FTRIM. At 50 eV, the calculation was repeated using both generator A and generator B (see **Figure 1**) to show that the results did not depend on the generator, just on the dimension. Finally, a comparison is made with a molecular dynamic simulation at 10 eV. The similarity of those results shows that FTRIM can be used with some confidence even at low energies. Comparisons of predicted reflection to experiment are not possible because reflection measurements have not been done in this energy range. The reflected particles come off neutral and are very difficult to detect. A better comparison to experiment can be made when sputtering is considered.

Figure 2a shows the FTRIM prediction [6] for physical sputtering of 300 eV H on C and normal incidence and at 60° incidence. Two experimental points [7] are also shown where the fractal

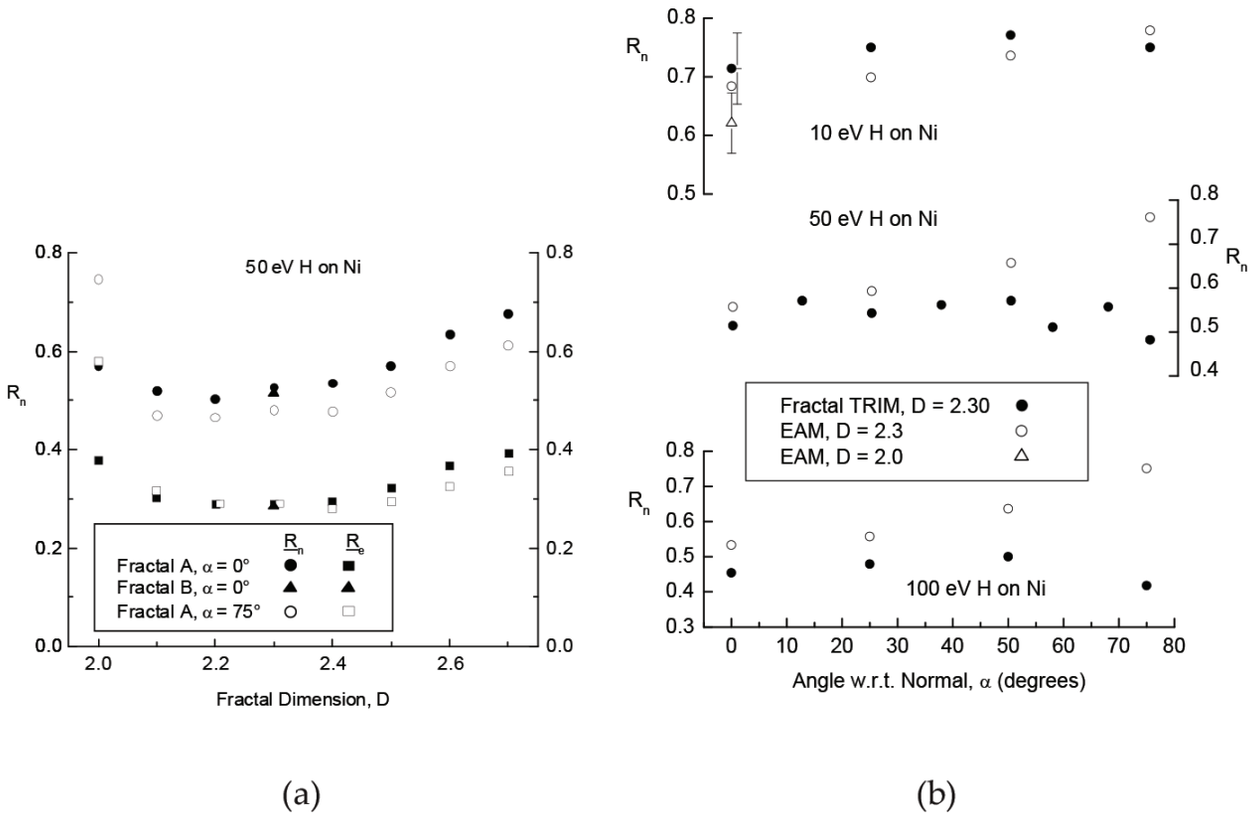

Figure 1. (a) R_n and R_e, particle and energy reflection coefficients, versus fractal dimension D for normal incidence ($\alpha = 0°$) and grazing incidence ($\alpha = 75°$) for three different surfaces. H is incident on Ni at 50 eV. The error bars are the size of the data points. Note the large drop-off of R at the grazing incidence when D is greater than 2.00. (b) Reflection coefficients for 10, 50, and 100 eV H on Ni as a function of the incident angle (with respect to normal, w.R.T.) for a fractal Ni surface with dimension 2.30. Planar TRIM results and a molecular dynamics calculation using the embedded atom method (EAM) are also shown. Note that planar TRIM predicts reflection at the grazing incidence to be two to three times more likely than the fractal TRIM results. Statistical errors in the fractal and planar TRIM reflection coefficients are generally less than 5%.

dimension of the surface is known [8] and the agreement is very good. **Figure 2b** shows the sputtering yield of 100 eV C on C as a function of the fractal dimension for a variety of incident angles. Initially, adding roughness increases the yield. This is due to the ability of the incident ions to knock off target atoms, which may protrude from the surface. Therefore, as expected, higher angles of incidence show an even greater rise in sputtering. The sputtering goes down for a very high roughness because the sputtered atoms are recaptured by overhanging features. Planar TRIM results are also shown. Note that the effective surface roughness for planar TRIM is only 2.00 at the normal incidence. The algorithm described earlier picks the location of the initial collision partner. If that partner would be above the surface, it is not used. The set of initial collision partner locations has a nonuniform depth distribution if the incident angle is not perpendicular to the surface. An equivalent roughness to the fractal surfaces can then be assigned. FTRIM predicts less sputtering than TRIM at higher angles of incidence and more sputtering at normal incidence. This result is significant, in that the realistic surfaces that evolve due to plasma-induced erosion and re-deposition in a fusion device with enhanced roughness will likely impact the amount of net erosion and reflected energy of fuel particles that can influence the operational regimes in these devices.

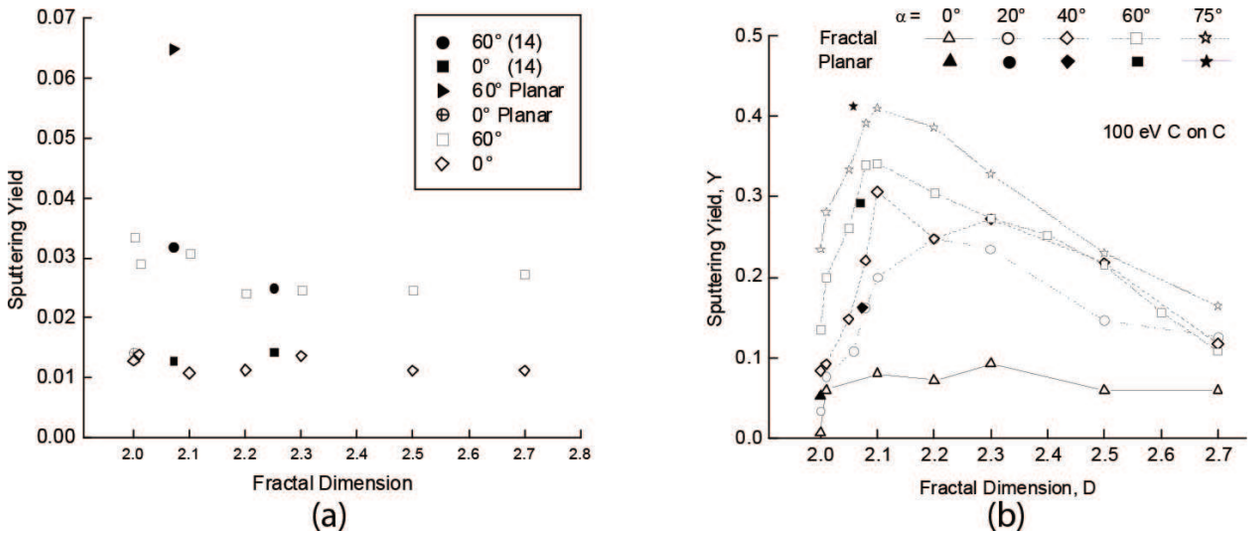

Figure 2. (a) Sputtering yield of 300 eV H on C as a function of fractal dimension, D. The D of the experimental points by Haasz et al. [7] is based on the work by Avnir et al. [8]. (b) Sputtering yield of target material as a function of the fractal dimension and the angle of incidence for 100 eV C incident on a C target. The normal incidence is 0°. Statistical errors in the yield are generally less than 5%.

3. Sputtering from plasma-material interactions

3.1. Solid-phase sputtering of fusion-relevant materials

One of the fundamental interactions between plasmas and material surfaces is physical sputtering or ion-induced desorption. The plasma edge magnetic field lines in a magnetic fusion device such as a tokamak directs energetic charged particles to gyro-orbit and bombards surfaces at both incident angle distributions and energy distributions that are linked with the operational regime of the fusion device. Therefore, the average incident angle will be close to 45° with respect to the normal and low-incident-particle energies. Fusion device PMI can be divided between two overall types of solid-state materials: low-Z materials and high-Z materials. There is a trade-off in the selection of materials for the first wall in fusion devices. The cooling of the plasma due to eroded particles from the device wall material goes as ~Z^2. Therefore, low-Z materials are attractive; however, these materials tend to have low surface binding energies, which result in high-sputter yields. The sputtering yield is defined as the ratio of flux of sputtered particles over the flux of incident energetic particles. High-Z materials can sputter orders of magnitude lower than low-Z materials; however, this must be balanced against plasma cooling losses. As stated earlier in fusion devices, the material surface will evolve where roughness can become significant [9–11].

3.1.1. Low-Z material sputtering by light incident particles

Low-Z material sputtering is relevant to plasma-surface interaction physics in fusion devices from the standpoint of minimizing fractional impurity levels in fusion plasmas [12]. **Figure 3a** shows experimental measurements and VFTRIM-3D simulations of sputtering yields for Li, He, and D bombardment at 45° incidence on deuterium-treated solid-phase lithium [13].

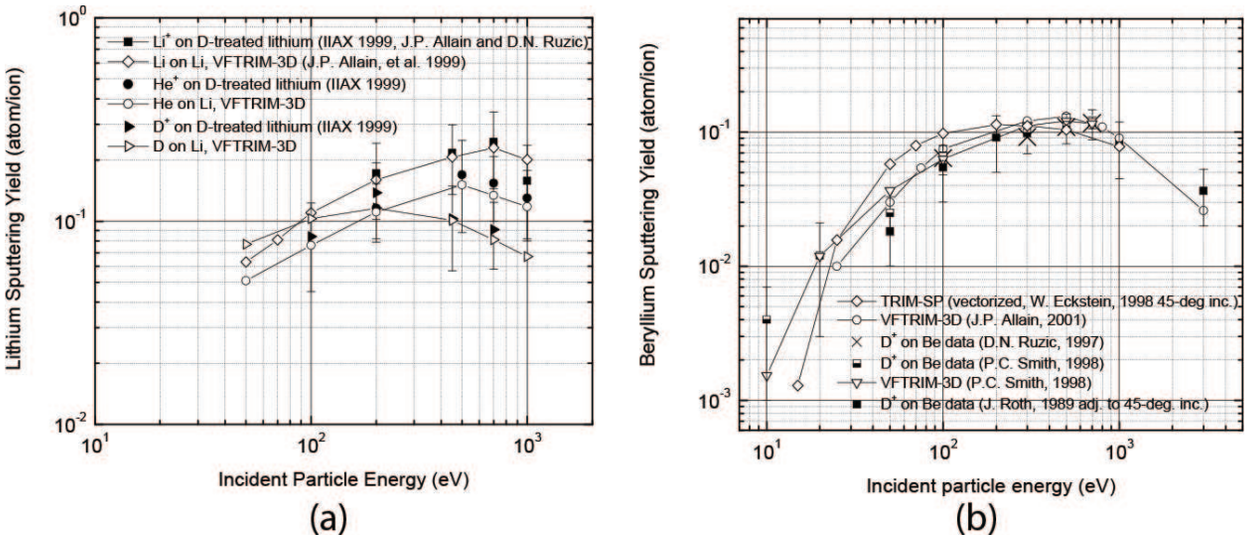

Figure 3. (a) Experimental and VFTRIM-3D simulation data for li, D, and he bombardment of solid-phase D-treated lithium at 45° incidence. (b) Experimental and simulation results for D^+ bombardment of D-treated beryllium at 45° incidence. Normal incidence data are adjusted to 45° using Yamamura's formula for oblique incidence.

Experimental data were taken at the Ion-surface Interaction Experiment (IIAX) facility, which is an ion beam experimental device able to measure, among other things, physical sputtering yields for low-energy, light-particle interaction. The data is done at 45° incidence, based roughly on the average angle of incidence a sheath-accelerated, gyrating particle makes where the magnetic field lines cross the divertor plates at oblique incident angles [14].

Computational runs were modeled using a surface, which consisted of 50 a/o Li and 50 a/o D, consistent with deuterium concentration measurements [15]. The model used a surface binding energy of 1.68 eV based on the heat of sublimation for solid lithium. The value of 1.68 eV for the surface binding energy of Li has been measured in plasma-surface interaction experiments in PISCES-B [16]. The bond energy (*BE*)—the energy to break a bond in the bulk—was taken as $BE = 0.1\ SBE$. Deuteration of the solid lithium surface is done with a deuterium plasma from a hollow cathode source with a flux of 10^{16} ions/cm^2/s for 20 min. This flux is sufficient to saturate the surface and have enough atomic percentage of deuterium to assume a 50/50 composition at the surface over a range at least the depth of origin of sputtered species.

The sputtering yield behavior shown in **Figure 3a** is as expected. Due to the ineffective transfer of energy between hydrogen isotopes and lithium compared to helium or lithium itself, lithium sputtering due to hydrogen isotopes is relatively low. For the same incident energy, hydrogen atoms will penetrate farther into the lithium bcc lattice. Therefore, hydrogen isotope bombardment of lithium will reach a maximum sputtering yield at a lower incident energy than for helium or lithium bombardment. At greater energies, the penetration depth is deep enough that the net backward momentum distributed to surface atoms is not sufficient to overcome the surface binding energy, and thus the lithium-sputtering yield begins to decrease. Self-sputtering of lithium will be discussed in Section 4.2, following which we discuss lithium sputtering from deuterium and helium bombardment.

VFTRIM-3D simulation results for deuterium bombardment are shown in **Figure 3a** with open triangles (pointing toward right), while closed triangles represent IIAX data. The solid line serves to guide the eye. The experimental and simulated yields versus incident-particle energy diverge with a decreasing energy primarily in the low 10–100 eV range, although the error bars are relatively large. At these lower energies, the range of incoming deuterium ions extends only to a few monolayers. Over the period of the dose, the surface may be enriched with more deuterium, leading to a lower amount of lithium sputtered than predicted. In addition, at these lower energies, the influence of surface roughness on the sputtering yield is enhanced. This occurs due to D atoms segregating to protruding regions of the surface where the net attractive force to the bulk/surface goes as r^{-3} (where r is the distance from the surface) [16] and thus the effective binding energy to the surface for these atoms drops. Studies have shown that hydrogen atoms will tend to segregate to interstitial sites in a metal lattice [17–19]. In addition, the diffusion of hydrogen atoms has been measured in lithium experiments investigated by Sugai [15]. Such diffusion is not modeled by TRIM-SP, only that a continuous distribution of D atoms exists in the lithium bcc lattice. Thus, the ability for diffusion and segregation of deuterium atoms around the protruding regions of the lithium surface adds to the probability that less amount of lithium is sputtered since a larger amount of deuterium is preferentially sputtered. The yield reaches a maximum around 200–300 eV. At an incident-particle energy of 200 eV, where the yield is a maximum, the mean sputtered energy of lithium atoms is 9.0 eV as predicted by TRIM-SP.

Figure 3a also shows the experimental and computational results for He^+ bombardment of D-treated lithium at 45° incidence. The line with open circles represents the TRIM-SP simulation data. The solid circles represent IIAX data. The prediction made by the computational model falls within the experimental error. The functional behavior shows a maximum of the sputtering yield of lithium at 500 eV. The decrease of lithium sputtering due to deuteration of lithium is stronger for helium bombardment than for deuterium. This is due to the effective transfer of energy from the incident hydrogen isotopes to the implanted deuterium atoms, leading to a relatively larger net momentum imparted to lithium surface atoms.

Beryllium sputtering has been studied quite extensively ranging from ion-beam experiments to experiments from magnetized linear plasma devices, such as PISCES-B [20–29]. **Figure 3b** shows both experimental data and simulation data for deuterium bombardment of beryllium. Experimental data are shown in x's and half-filled squares for IIAX data by Ruzic et al. [24], filled squares for Roth et al. [20], which are adjusted to 45° incidence by an empirical formula given by Yamamura et al. [30]. The empirical relation is shown as Eq. (1) and the fitting parameters used are obtained from the quoted reference for the factors f and α_{opt} where α_{opt} is the nominal incidence angle at maximum yield [31]. Simulated data for TRIM-SP are shown in open circles and triangles [23]. TRIM-SP simulation is shown with open diamonds for 45° incidence [32]

$$\frac{Y(E_o,\alpha)}{Y(E_o,\alpha=0)} = \frac{\exp\left(f\left[1-\frac{1}{\cos\alpha}\right]\cos\alpha_{opt}\right)}{\cos^f\alpha} \tag{1}$$

TRIM-SP simulations were done for a fixed surface binding energy of 3.38 eV, which is the heat of sublimation for beryllium. Since in the IIAX experiment, beryllium was saturated with

deuterium at room temperature, a surface composed of a D/Be ratio of 0.33 was used based on saturation experiments [33]. VFTRIM-3D simulations use a vectorized version of TRIM-SP known as TRVMC, which uses a binding energy of 1 eV for hydrogen isotopes [32] and beryllium's heat of sublimation. This binding energy was also utilized by TRIM-SP for consistency.

The data shown in **Figure 3b** show a maximum between 300 and 500 eV, closely resembling BeO data taken by Roth et al. [20]. Beryllium has a high affinity for oxygen at room temperature, thus the surface binding energy is effectively increased, reducing the sputtering yield. In addition, deuterium-treated surfaces effectively decrease beryllium sputtering due to preferential sputtering of embedded deuterium atoms. As a consequence, the beryllium sputtering yield from deuterium-treated surfaces measured in IIAX is predicted well by VFTRIM-3D simulations. TRIM-SP simulations do not account for deuterium treatment, and thus their yields are higher than anticipated, coincidently matching VFTRIM-3D results. If deuterium saturation was used by TRIM-SP modeling, beryllium sputtering would be effectively decreased, thus not predicting the experimental data in IIAX. The ability for VFTRIM-3D to effectively model surface roughness also leads to the high predictability of experimental data both in IIAX and from Roth et al. [20].

3.1.2. High-Z material sputtering by light incident particles

High-Z material sputtering will be discussed for the cases of tin and tungsten sputtering. High-Z material sputtering for refractory materials such as tungsten is attractive due to its relatively low-sputtering yield and high-sputtering threshold. However, due to the plasma low tolerance for high-Z impurities due to radiation losses, impurity levels must remain low, $<10^{-4}$ (ratio of densities) in fusion plasmas [11]. Other high-Z materials such as tin are attractive from the standpoint of low-sputtering yield, relatively high-sputtering threshold, high thermal conductivity, and the potential for tin to be used as a liquid plasma-facing material due to its low melting point and low vapor pressure. For experimental data at normal incidence, the empirical formula (Eq. (1)) by Yamamura et al. was used as in the case for beryllium.

Figure 4a shows the results for TRIM-SP simulation of tin sputtering. The VFTRIM-3D simulations are done for a surface binding energy equal to the heat of sublimation of tin, 3.12 eV. The data presented are as expected with helium bombardment, leading to a larger tin sputtering than deuterium bombardment due to an effective energy transfer. A maximum for deuterium bombardment is reached at a slightly lower incident energy than for helium bombardment. The argument for when this maximum yield is reached is the same as for tungsten, noting that in addition for heavy materials, the penetration depths of deuterium and helium at low energies will be quite similar and thus their maxima remain close. Tin shows promise, in that its sputtering yield at energies ranging from 100 to 400 eV is about a factor of five less than beryllium sputtering. However, one would have to contend with radiation losses from tin's high Z equal to 50.

Figure 4b shows the experimental and VFTRIM-3D simulation results for tungsten self-sputtering as well as tungsten sputtering from deuterium and helium bombardment. The experimental data are for normal incidence taken by Eckstein et al. at low energy and has been

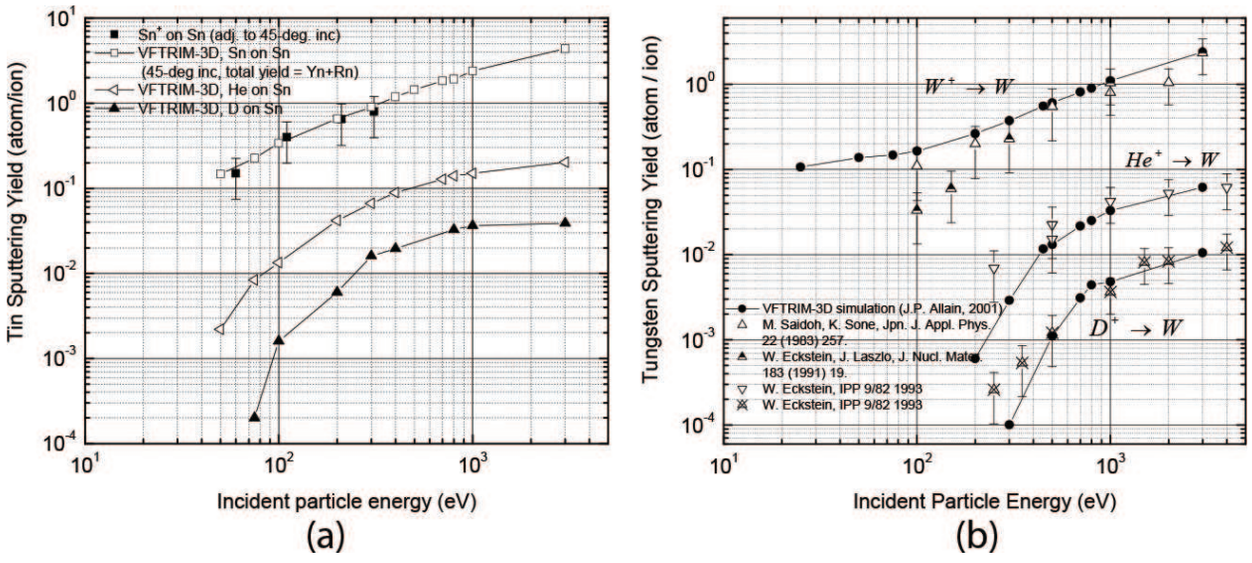

Figure 4. (a) Experimental and VFTRIM-3D simulation of tin sputtering by D, he, and Sn incident particles at 45° incidence. Normal incidence data are adjusted to 45° using Yamamura's formula (Eq. (1)) for oblique particle incidence. (b) Experimental and VFTRIM-3D simulation of tungsten sputtering by D, he, and self-ions at 45° incidence. Normal incidence data are adjusted to 45° using Yamamura's formula (Eq. (1)) for oblique particle incidence.

adjusted to 45° incidence for comparison [11]. TRIM-SP simulations were done for tungsten with a surface binding energy equal to its heat of sublimation of 8.68 eV. A mass density of 19.3 g/cm^3 was used in the simulation as well.

The VFTRIM-3D simulation predicts the experimental data reasonably well within the error bars. Helium bombardment shows a lower-sputtering threshold and larger yields compared to deuterium bombardment as expected from a lower mass ratio and a better energy transfer. Although the data are not shown for larger energies than 3 keV, the maximum tungsten-sputtering yield is expected at a lower incident energy for deuterium bombardment than for helium bombardment. This is due to the longer range of deuterium atoms in tungsten compared to that of incident helium, depositing less energy near the surface and thus turning the sputtering yield curve at a lower incident energy than helium.

3.1.3. Effect of deuterium saturation on lithium and beryllium sputtering

The sputtering yield of lithium and beryllium decreases with deuterium saturation of the surface. This is due to preferential sputtering of deuterium atoms over lithium or beryllium atoms when bombarded by incident energetic particles. In the case of deuterium treatment for beryllium target, an extensive review has been presented in previous work and is only referenced here [10, 24, 27]. The net effect of embedded deuterium atoms is the effective reduction of the beryllium and lithium-sputtering yield as demonstrated by VFTRIM-3D simulations, shown in **Figure 5a** for deuterium bombardment. The simulations maintained the surface binding energy fixed at 3.38 eV. The level of deuterium saturation is that described earlier with a D/Be ratio of 0.33. For lithium sputtering, deuterium saturation is modeled with a D/Li ratio of 0.5 as discussed earlier. The lithium surface binding energy is kept fixed at 1.68 eV.

The effect of deuterium saturation on beryllium sputtering is a bit stronger for helium bombardment (not shown here) than for deuterium bombardment. This is due to the effective energy transfer from the incoming deuterium to the embedded deuterium atoms in beryllium and lithium. This effect, however, is lessened with a lower amount of deuterium in the beryllium or lithium lattice. Therefore, the energy dependence for a given deuterium saturation level in a material cannot be simply determined from the energy dependence at 0% saturation by a constant multiplication. Similar results are found for lithium sputtering except for larger yields and a lower-sputtering threshold mostly due to a better energy transfer from deuterium and helium atoms to lithium target atoms.

Figure 5b further shows the importance of deuterium treatment on the *measured* absolute sputtering yield of solid lithium (i.e., IIAX experiments). **Figure 5b** shows experimental and VFTRIM-3D simulation results for He^+ bombardment on D-treated and non-D-treated lithium at 45° incidence. The figure plots the energy dependence of the absolute sputtering yield of lithium in atoms per incident ion. The lithium-sputtering yield functional behavior of the non-D-treated lithium target is shifted toward a maximum at higher energies (~1000 eV) for one of the experimental cases. The VFTRIM-3D results begin to diverge the experimental data at energies above 500 eV. In addition, the computational model used for the non-D-treated data is based on a mechanism for channeling energy from subsurface layers to the top layer [23]. The simulation model used to predict the D-treated data does not utilize this mechanism. This result implies that the absence of deuterium atoms at interstitial sites of the lithium bcc lattice allows for atoms from deeper in the sputtering cascade to transfer their momentum up to surface layer atoms, thus contributing to more sputtering.

The D-treated lithium-sputtering yield is measured to be significantly lower than bombardment with no deuterium treatment. As explained earlier, preferential sputtering is expected for

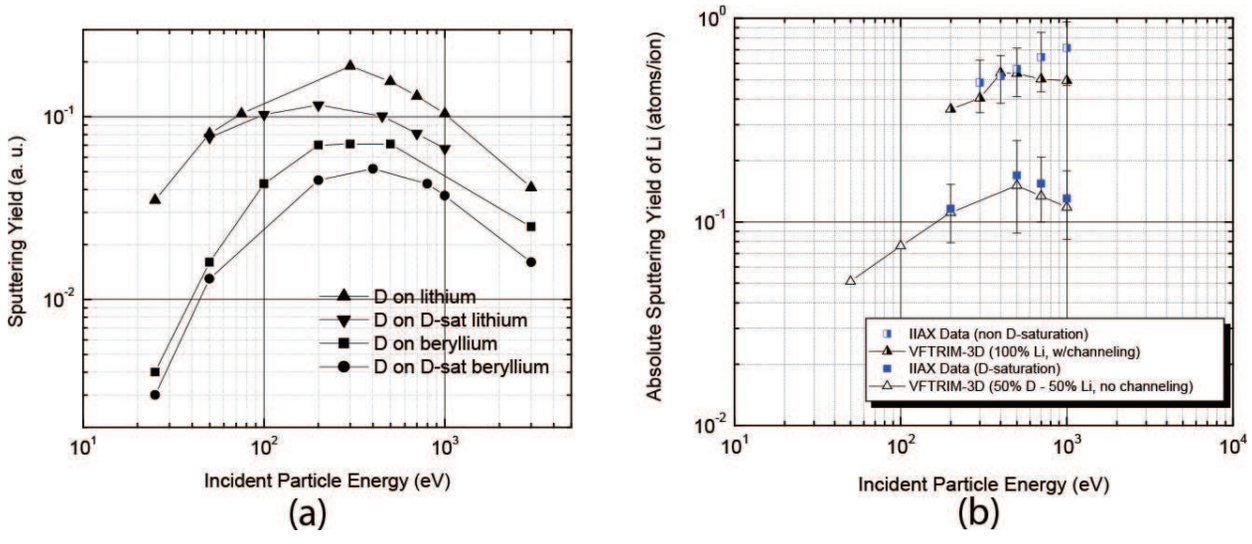

Figure 5. (a) VFTRIM-3D simulation of deuterium sputtering of D-treated and non-D-treated lithium and beryllium at 45° incidence. Deuterium saturation levels for lithium are 50% D/li, and for beryllium, 33% D/be. These are levels of saturation, which mimic those expected from PMI interactions in magnetic fusion devices at the wall boundary. (b) Energy dependence of 45° incidence he^+ bombardment on non-D-treated and D-treated solid lithium measurements and VFTRIM-3D simulation.

the lightest component and for the least bound species. The deuterium is sputtered preferentially and the surface, in time, is enriched in lithium. However, at doses in IIAX and doses found in typical plasma-facing conditions in tokamaks, the one-to-one ratio of lithium matrix atoms and saturating-deuteride species are kept over at least the depth of origin of sputtered species as a constant flux of deuterium atoms impinges on the lithium sample and a source of implanted deuterium atoms segregates to the surface over the time of dose [34–36].

Another factor is the competition between preferential sputtering on the one hand, and mixing or segregation on the other [37, 38]. These latter effects are less pronounced here since we have a surface that is "soaked" with deuterium atoms and not an alloy composed of deuterium and lithium constituents. Therefore, preferential sputtering mechanisms are justified as a viable interpretation. The binding of deuterium and lithium atoms is less likely than deuterium atoms penetrating and sitting at interstitial sites in bcc lithium.

3.1.4. Self-sputtering

Self-sputtering at the plasma boundary in fusion devices will occur for impurities, which have been injected into the plasma, are ionized, and return to strike solid surfaces at the wall or divertor regions. The momentum transfer between like masses is extremely effective due to maximum energy transfer, leading to increased sputtering and potentially diluting the plasma with impurities. There are two components in self-sputtering that must be considered. One is the erosion component due to physical sputtering and the other is the reflection of the incident particle into the plasma. Since both sources cannot be distinguished from each other, except their average particle energy, these sources must be added to obtain the total amount of particles injected into the plasma. **Figure 6a** shows the self-sputtering yield (sputtering +

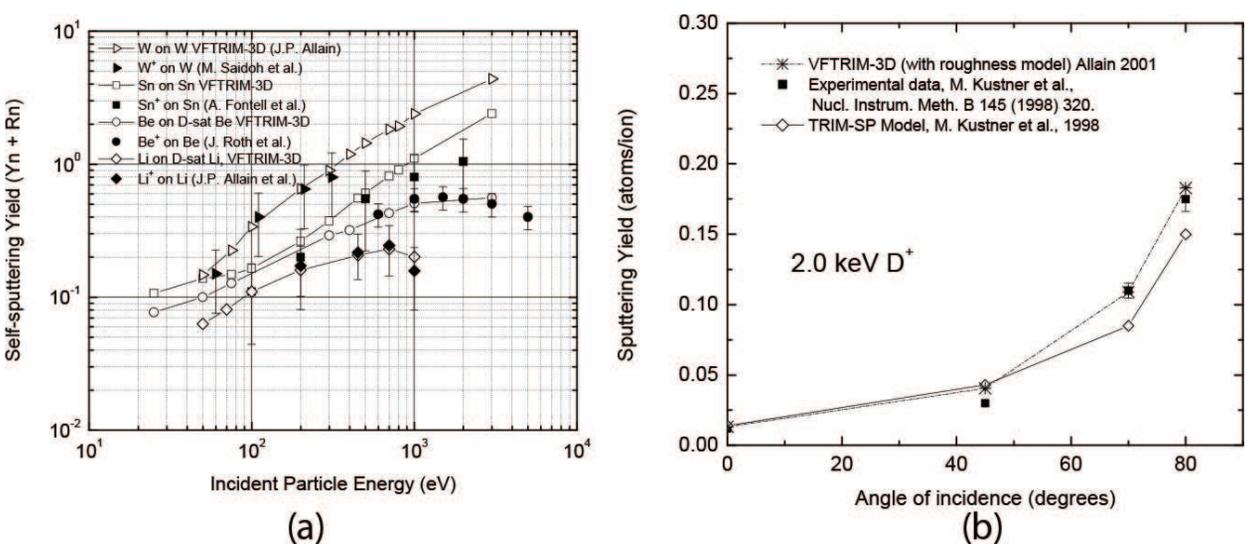

Figure 6. (a) Self-sputtering experimental and simulation yields (total = reflection and sputtering for TRIM-SP simulations) of tungsten, tin, beryllium, and lithium at 45° incidence. Normal incidence data are adjusted to 45° using the Yamamura formula for oblique particle incidence. (b) VFTRIM-3D, TRIM-SP and experimental data of 2 keV D^+ bombardment of graphite versus particle angle of incidence.

reflection) for the cases of tin, lithium, tungsten, and beryllium at 45° incidence. Normal incidence data are adjusted to 45° incidence by Yamamura's empirical formula (Eq. (1)) for oblique particle incidence.

Self-sputtering of tungsten and tin is simulated by VFTRIM-3D and compared with experimental data in **Figure 6a**. Due to the highly efficient transfer of energy process in self-sputtering, tungsten results in the largest yield still increasing at 3 keV. Tin self-sputtering [34–39] is shown to have a slightly lower-sputtering yield close to beryllium self-sputtering for energies up to 1 keV within experimental uncertainty. Beryllium self-sputtering is elaborated on in several papers [20–22]. The beryllium self-sputtering yield is found to have a maximum at about 1.2 keV. The data are predicted quite successfully as surface roughness is modeled by VFTRIM-3D. This is an important point that will be elaborated on in the next section regarding the dependence of the sputtering yield on the angle of incidence of the bombarding particle and the fact that in fusion devices PMI results in evolving surfaces that can roughen over the time scale of plasma-induced modification and operation.

Figure 6a also shows the experimental and computational results for lithium self-sputtering at 45° incidence. Computational data using TRIM-SP for incident-particle reflection are also included in the self-sputtering yield calculated. The experimental results are surprising. The self-sputtering yield of solid lithium maximizes at 700 eV to a value of 0.245 ± 0.100 atoms/ion. This is considerably lower than the values predicted by László and Eckstein [40]. There are two main reasons why the calculated values by László and Eckstein are significantly greater than our measured results. The computational model used by J. László et al. used the TRIM-SP, which assumes a smooth surface and neglects surface roughness. Second, the model does not utilize a compositional component to incorporate the effect of deuterium implantation at interstitial sites of the lithium sample as discussed in the previous section.

Within the experimental error, the simulation predicts the functional behavior of the sputter yield, except at higher energies ($E \geq 800$ eV) where the two begin to slightly diverge. This is due to a shorter mean range of the incident lithium ion in solid lithium compared to D or He. Thus, a large percentage of its kinetic energy is distributed among the top-most surface deuterium atoms, which lead to a preferentially larger deuterium erosion and a reduction of lithium sputtering. The fact that lithium self-sputtering is significantly reduced due to deuterium saturation of the surface is encouraging for its use as a potential plasma-facing component.

3.2. Sputtering yield dependence on angle of incidence

As discussed in the introductory sections of this review, the effect of roughness on the sputtering yield of materials is enhanced with an increase in the angle of incidence. **Figure 6b** shows the angle of incidence dependence of graphite sputtering by 2-keV incident deuterium ions. As the angle of incidence is increased, the effect of surface roughness is enhanced and thus simulation using TRIM-SP better predicts the data very well compared to using a smooth surface simulation with TRIM-SP [41]. **Figure 7a** demonstrates this effect for beryllium self-sputtering as well. Two sets of experimental data [10, 21] are plotted with VFTRIM-3D and TRIM-SP simulations for 1-keV beryllium self-sputtering. Again in this case, the experimental

data are predicted successfully for VFTRIM-3D modeling roughness. The scatter in the experimental data at high angles of incidence is due to a variety of roughness levels in the materials as well as the creation of surface roughness in the course of ion bombardment.

The lithium self-sputtering yield for deuterium-treated and non-deuterium-treated surfaces is shown in **Figure 7b**. The dependence of the lithium-sputtering yield on the angle of incidence is also shown for two incident energies, 100 and 500 eV. Due to the importance of self-sputtering runaway, a thick black (red) line indicates unity lithium-sputtering yield. Unity self-sputtering means the sputtered flux is greater than the incident-particle flux and thus the potential for a runaway condition, which results in enhanced amounts of target material being eroded, re-ionized, and re-deposited with an impact on fusion device operation. The dependence of the lithium-sputtering yield on the angle of incidence is strong for higher oblique angles. This is due to the decrease in the penetration length of the incident bombarding atom and consequently greater energy deposition near the surface, increasing the probability to sputter. For deuterium-treated surfaces, the lithium-sputtering yield is lower than non-deuterium-treated surfaces at all angles of incidence shown and the given incident energies.

The lithium yield due to 500-eV incident lithium atoms on deuterium-treated lithium is slightly lower than the case for 100-eV lithium on non-deuterium-treated lithium. This is due to preferential sputtering of deuterium atoms playing a large role in reducing the lithium-sputtering yield even at higher energies. At 500 eV, lithium penetrates farther and thus the resulting lithium yield is lower. However, at larger angles of incidence, the energy deposition increases even for the case of deuterium-treated lithium, thus the yield crosses the low energy curve for non-deuterium-treated lithium. For the high-energy case with no deuterium coverage, we find that self-sputtering runaway is reached at a lower angle of incidence than for deuterium-treated lithium. This occurs at an angle of incidence of about 55°, while with

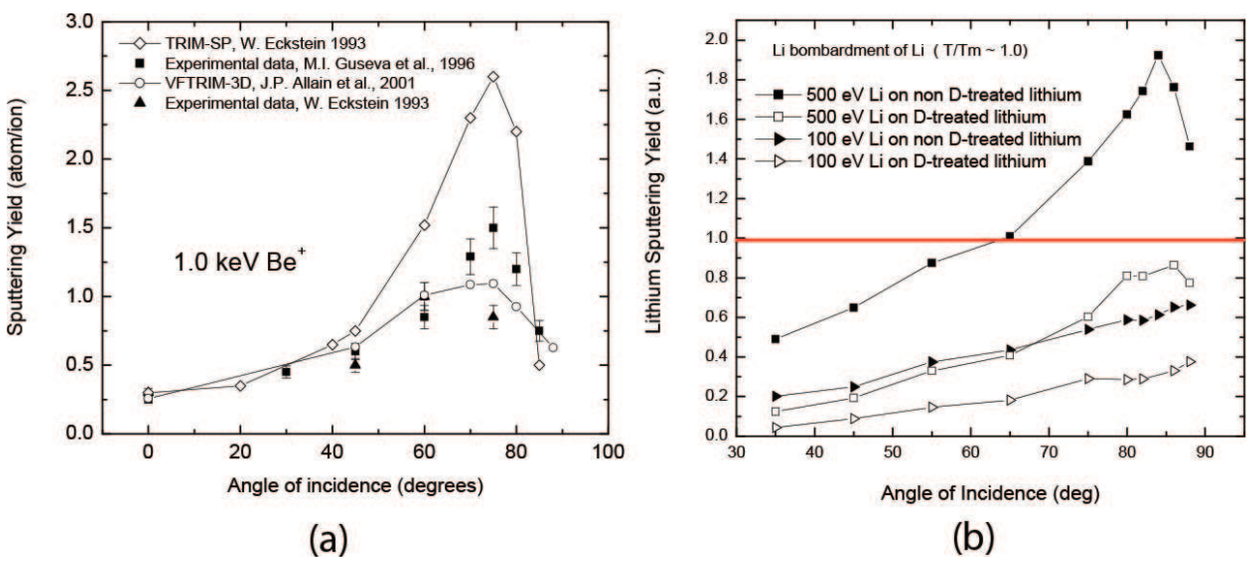

Figure 7. (a) VFTRIM-3D, TRIM-SP, and experimental data of 1 keV be$^+$ bombardment of beryllium against nominal particle angle of incidence. (b) Self-sputtering yield from lithium surface at about 200°C, for deuterium-treated and non-deuterium-treated lithium. TRIM-SP simulations are done for 45° incidence and 100 and 500 eV incident-particle energies.

deuterium-treated surfaces, the lithium yield remains under unity up to about 70° incidence at 500-eV incident-particle energy. This has some important implications. If one can maintain a one-to-one deuterium to lithium coverage, self-sputtering runaway of lithium could be dramatically reduced even for incident particles at high energies. This is important since deuterium-absorbed lithium plasma-facing surfaces give rise to low-recycling plasma regimes at the edge [42]. The comparison of the sputtering yield dependence on the incident angle *and* differences of incident-particle energy are illustrated in **Figure 8**. **Figure 8** shows the lithium sputter yield for both D-saturated and non-D-saturated surface conditions sputtered by 100 and 1000 eV D atoms. Notice that the enhancement with an incident angle decreases with a decreasing incident energy and in fact become equal at 60° incidence, which means that the energy deposition is predominant on the surface and only D saturation could significantly decrease the sputtering.

3.3. Secondary ion sputtering fraction in lithium sputtering

Another very important property in PMI is the surface charge density and the role of charge dynamics when sputtered atoms are released from the surface. The secondary ion sputtering fraction, defined as the fraction of ions to neutrals sputtered from the incident ions, has been measured for lithium sputtering by bombardment of D^+, He^+, and Li^+ at low energies and oblique incidence [13]. Such a measurement is important since in a fusion device, plasma-sputtered ions will immediately return to the surface due to the sheath potential and thus not

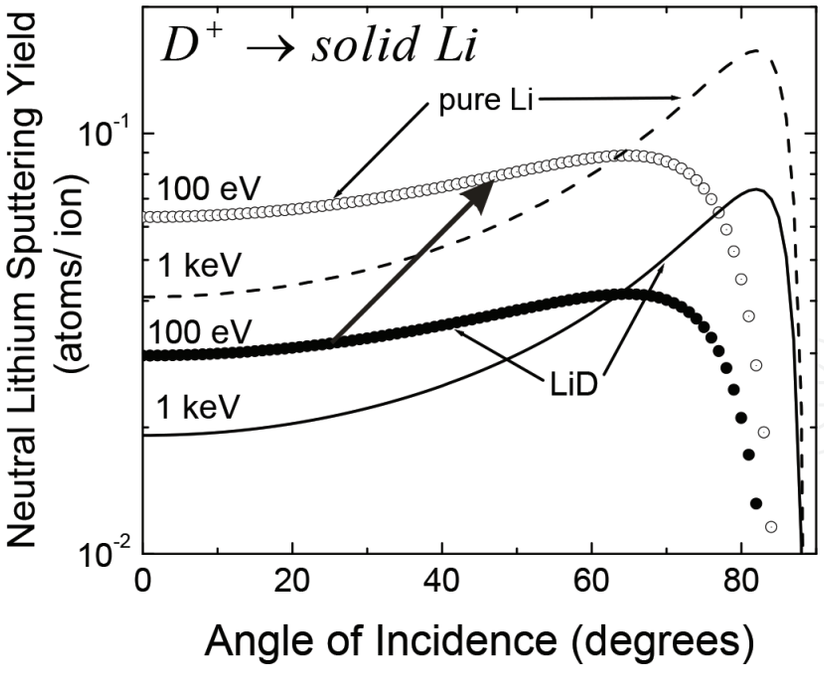

Figure 8. Lithium-sputtering yield versus angle of incidence using the Bohdansky-Sigmund-Yamamura (BSY) model. Open circles: 100 eV D on solid pure (100%) lithium; filled circles: 100 eV D on solid LiD (50% D-li); dashed line: 1 keV D on solid pure li; solid line: 1 keV D on solid LiD. As a deuterium-treated sample loses D near the li surface, the lithium-sputtering yield begins to increase and approaches the pure li yield. This is shown by the large arrow pointing in the direction of li-sputtering increase.

contribute to the sputtering yield. The secondary ion sputtering fraction does not vary significantly in the range of 500–1000 eV. The fraction of sputtered atoms in the ionic state is measured to be about 65% or two out of three sputtered atoms come out as ions. The dependence of the secondary ion fraction has been linked with the combination of chemical potential and work function of a surface with alkali metals having the highest yields.

4. Conclusion

An introduction to plasma-material interactions in fusion devices was provided in this chapter. The effects of varying surface roughness were described and the use of fractal dimensions as a viable model for simulating PMI of realistic surfaces. Physical sputtering and particle reflection were selected as primary mechanisms of PMI. Simulations and experimental data of low-Z and high-Z materials were provided. Fusion relevant ion-surface interactions for candidate materials were presented. These included combinations of D, T, and He on Li, Be, C, Sn, and W with and without D-saturation of the surfaces.

Results show that surface roughness is an important effect that must be accounted for in reflection and sputtering measurements, especially at low-incident-particle energies and oblique incidence. Low-Z materials such as lithium and beryllium suffer from low-sputtering thresholds, however, maintaining fairly low self-sputtering yields. High-sputtering thresholds on the other hand characterize high-Z materials but maintain high self-sputtering yields even at low bombarding energies. Oblique incidence is important to consider due to the strong dependence of sputtering on the incident-particle angle. Deuterium saturation of low-Z materials such as lithium or beryllium effectively reduces sputtering. Moreover, lithium has a high secondary ion-sputtering fraction, thus leading to an even lower-sputtering yield.

Acknowledgements

We acknowledge our funding sources DOE-OFES grant DE-SC0010717. To learn more about the Center for Plasma-Material Interactions and the Radiation Surface Science and Engineering Laboratory, visit our sites: (http://rssel.engineering.illinois.edu) and (http://cpmi.illinios.edu).

Author details

Jean Paul Allain* and David N. Ruzic

*Address all correspondence to: allain@illinois.edu

Department of Nuclear, Plasma and Radiological Engineering, Center for Plasma-Material Interactions, University of Illinois at Urbana-Champaign, Urbana, IL, USA

References

[1] Bringa EM. The Astrophysical Journal. 2008;**662**(1):372

[2] Greenberg JM. Surface Science. 2002;**500**:793

[3] Biersack J, Eckstein W. Applied Physics A. 1984;**34**:730

[4] Avnir D, Farin D, Pfeifer P. Nature. 1984;**308**:261

[5] Ruzic DN, Chiu HK. Journal of Nuclear Materials. 1989;**162-164**:904

[6] Ruzic DN. Nuclear Instruments and Methods B. 1990;**47**:118

[7] Haasz AA, Davis JW, Wu CH. Journal of Nuclear Materials. 1989;**162-164**:915

[8] Avnir D, Farin D, Pfeifer P. The Journal of Chemical Physics. 1983;**79**:3566

[9] Shaheen MA, Ruzic DN. Journal of Vacuum Science and Technology A. 1993;**11**:3085

[10] Eckstein W, Laszlo J. Journal of Nuclear Materials. 1991;**183**:19-24

[11] Federici G et al. Nuclear Fusion. 2001;**41**:12

[12] Stangeby PC. The plasma boundary of magnetic fusion devices. In: Scott P, Wilhelmsson H, editors. Plasma Physics Series. Boston: Institute of Physics Publishing; 2000

[13] Allain JP, Ruzic DN. Nuclear Fusion. 2001;**41**:12

[14] Chodura R. Physics of plasma wall interactions in controlled fusion. In: Post DE, Behrisch R, editors. NATO ASI Series B: Physics. Vol. 131. New York: Plenum Press; 1984. (DeWald AB, Bailey AW, Brooks JN, Physics Fluids 30, (1987) 267

[15] Sugai H. Vacuum. 1996;**47**(6-8):981-984

[16] Doerner RP et al. Journal of Nuclear Materials. 2001;**290-293**:166-172

[17] Myers SM, PM Richards WR. Wampler. Journal of Nuclear Materials. 1989;**165**:9

[18] Wampler WR. Journal of Nuclear Materials. 1984;**122-123**:1598

[19] Haasz AA, Davis JW. Journal of Nuclear Materials. 1997;**241-243**:1076

[20] Roth J, Eckstein W, Guseva MI. Fusion Engineering and Design. 1997;**37**:465-480

[21] Guseva MI et al. Journal of Nuclear Materials. 1997;**241-243**:1117-1121

[22] Hechtl E, Roth J, Eckstein W, Wu CH. Journal of Nuclear Materials. 1995;**220-222**:883-885

[23] Smith PC, Ruzic DN. Nuclear Fusion. 1998;**38**(5):673-679

[24] Ruzic DN, Smith PC, Turkot RB Jr. Journal of Nuclear Materials. 1997;**241-243**:1170-1174

[25] Guseva MI, Suvorov AL, Korshunov SN, Lazarev NE. Journal of Nuclear Materials. 1999; **266-269**:222-227

[26] Doerner RP et al. Journal of Nuclear Materials. 1998;**257**:51-58

[27] Alimov VK, Chernikov VN, Zakharov AP. Journal of Nuclear Materials. 1997;**241-243**: 1047-1052

[28] Roth J, Eckstein W, Bohdansky J. Journal of Nuclear Materials. 1989;**165**:199-204

[29] Roth J. Journal of Nuclear Materials. 1987;**145-147**:87-95

[30] Yamamura Y, Itikawa Y, Itoh N. Nagoya University Institute of Plasma Physics Report IPPJ-AM-26; 1983

[31] Kustner M, Eckstein W, Hecthl E, Roth J. Journal of Nuclear Materials. 1999;**265**:22

[32] Eckstein W. IPP Report 9/117. 1998

[33] Brooks JN et al. Journal of Nuclear Materials. 1997;**241-243**:294

[34] Sigmund P. Nuclear Instruments and Methods B. 1987;**27**:1-20

[35] Falcone G, Sigmund P. Applied Physics. 1981;**25**:307

[36] Sigmund P. Matematisk-Fysiske Meddelelser - Kongelige Danske Videnskabernes Selskab. 1993;**43**:255

[37] Sigmund P, Oliva A. Nuclear Instruments and Methods B. 1993;**82**:269

[38] Sigmund P, Glazov LG. Nuclear Instruments and Methods B. 2000;**164-165**:453

[39] Fontell A, Arminen E. Canadian Journal of Physics. 1969;**47**:2405

[40] László J, Eckstein W. Journal of Nuclear Materials. 1991;**184**:22-29

[41] Kustner M, Eckstein W, Dose V, Roth J. Nuclear Instruments and Methods B. 1998:320-331

[42] Brooks JN, Rognlien TD, Ruzic DN, Allain JP. Journal of Nuclear Materials. 2001;**290-293**: 185-190

IntechOpen